

Comparing four hard-sphere approximations for the low-temperature WCA melting line

Cite as: J. Chem. Phys. 157, 034502 (2022); doi: 10.1063/5.0097593

Submitted: 29 April 2022 • Accepted: 27 June 2022 •

Published Online: 19 July 2022



View Online



Export Citation



CrossMark

Eman Attia,  Jeppe C. Dyre,  and Ulf R. Pedersen^{a)} 

AFFILIATIONS

Glass and Time, IMFUFA, Department of Science and Environment, Roskilde University, P.O. Box 260, DK-4000 Roskilde, Denmark

Note: This paper is part of the JCP Special Topic on Fluids Meets Solids.

^{a)}Author to whom correspondence should be addressed: ulf@urp.dk

ABSTRACT

By combining interface-pinning simulations with numerical integration of the Clausius–Clapeyron equation, we accurately determine the melting-line coexistence pressure and fluid/crystal densities of the Weeks–Chandler–Andersen system, covering four decades of temperature. The data are used for comparing the melting-line predictions of the Boltzmann, Andersen–Weeks–Chandler, Barker–Henderson, and Stillinger hard-sphere approximations. The Andersen–Weeks–Chandler and Barker–Henderson theories give the most accurate predictions, and they both work excellently in the zero-temperature limit for which analytical expressions are derived here.

Published under an exclusive license by AIP Publishing. <https://doi.org/10.1063/5.0097593>

I. INTRODUCTION

While systems of purely repulsive particles are rarely found in nature, they provide convenient models for both fluids and solids.¹ Examples are the inverse-power law (IPL) systems based on a homogeneous pair potential that varies with distance r as $(r/\sigma)^{-n}$ (in which σ is a length)^{2–5} and the exponential repulsive (EXP) pair potential that varies with distance as $\exp(-r/\sigma)$.^{6–8} The oldest and most important purely repulsive system is that of hard spheres (HS),^{9–12} which despite its simplicity provides a good zeroth-order model of realistic systems with both repulsive and attractive interactions.^{13–18} A purely repulsive system has a single fluid phase and no gas–liquid phase transition. In contrast, the symmetry-breaking liquid–solid transition is present in all purely repulsive systems. Because of the absence of a gas phase, the liquid–solid phase boundary here extends to zero temperature.

This paper studies the noted Weeks, Chandler, and Andersen (WCA) purely repulsive system,^{17–44} which is arrived at by cutting and shifting the Lennard-Jones (LJ) interaction at its minimum.¹⁷ In contrast to the IPL and EXP systems, the WCA pair potential has a finite range beyond which pair forces are zero, such as those of the HS system. At the cutoff, the WCA pair potential and pair forces are smooth, and at low temperatures, one expects HS approximations to apply because only insignificant “overlaps” are possible.

Thus, studies of the low-temperature melting line of the WCA system provide an excellent testing ground for comparing different HS approximations, which motivates the present study. Section II introduces the WCA system and the four HS approximations considered and gives a few simulation details. Section III details how we determined the WCA melting line by interface pinning and Clausius–Clapeyron integration. The predictions of the different HS approximations with regard to pressure and fluid/solid densities at melting are compared in Sec. IV. Finally, Sec. V provides a brief outlook.

II. THE WCA SYSTEM AND HARD-SPHERE APPROXIMATIONS

A. The WCA system

We consider mono-disperse systems. Let $\mathbf{R} = (\mathbf{r}_1, \mathbf{r}_2, \dots, \mathbf{r}_N)$ be the collective coordinate vector of N particles with mass m confined to the volume V (with periodic boundaries) and define the (number) density by $\rho \equiv N/V$. The potential energy $U(\mathbf{R})$ is assumed to be a sum of pair contributions,

$$U(\mathbf{R}) = \sum_{n>m} v(|\mathbf{r}_m - \mathbf{r}_n|). \quad (1)$$

Recall that the LJ pair potential is defined^{45,46} by

$$v(r) \equiv 4\epsilon[(r/\sigma)^{-12} - (r/\sigma)^{-6}] \quad (2)$$

in which ϵ has units of energy and σ units of length. The WCA pair potential (Fig. 1) is defined by cutting and shifting the LJ potential at its minimum, which leads to¹⁷

$$v(r) = 4\epsilon[(r/\sigma)^{-12} - (r/\sigma)^{-6}] + 1/4 \quad \text{for } r \leq r_c \quad (3)$$

and zero otherwise, where

$$r_c = \sqrt[6]{2}\sigma \approx 1.1225\sigma. \quad (4)$$

The WCA pair potential is purely repulsive since the pair force $-dv/dr$ is non-negative for all r 's, and it is smooth since both $v(r)$ and its first derivative are continuous (the second derivative is discontinuous at r_c , though). All quantities obtained by simulations are below reported in units derived from m , σ , ϵ , and the Boltzmann constant k_B .

Simulations of the WCA system were conducted using the RUMD software package version 3.5.⁴⁷ An initial configuration is first constructed by setting up $8 \times 8 \times 20$ face-centered cubic (FCC) unit cells, resulting in a system of $N = 5120$ particles. This initial configuration is then scaled uniformly to the desired density ρ . If a liquid configuration is needed, the crystal is melted in a high-temperature simulation. The Newtonian equations of motion are discretized using the leap-frog algorithm⁴⁸ with the temperature-dependent time step,

$$dt = 0.001 \frac{\sigma}{\sqrt{k_B T/m}}. \quad (5)$$

Simulations in the NVT ensemble⁴⁷⁻⁵¹ are realized using a Langevin thermostat with relaxation time given by

$$t_T = 0.2 \frac{\sigma}{\sqrt{k_B T/m}}. \quad (6)$$

For $Np_z T$ Langevin simulations,^{47,50,51} we used the same thermostat relaxation time and the barostat relaxation time,

$$t_p = 100 \frac{\sigma}{\sqrt{k_B T/m}}. \quad (7)$$

We have found that introducing this $1/\sqrt{T}$ scaling to the relaxation times²⁵ provides a simple way to ensure stability and efficiency of computations spanning four orders of magnitude in temperature (see Ref. 43 for a different approach). Note that in this way, the average number of steps needed to travel the distance σ for a thermal particle is the same at all temperatures. The model approaches hard spheres at low temperatures, and in effect, the interaction distance narrows. Thus, we expect that shorter time steps are needed for temperatures lower than those investigated here.

B. Hard-sphere approximations to the WCA system

Perturbation theories have proven successful for describing many fluids near freezing.^{1,15-25,52-66} The basic assumption is that the pair interaction can be written as

$$v(r) = v_0(r) + v_1(r) \quad (8)$$

in which $v_0(r)$ is the pair potential of some well-known reference system and $v_1(r)$ is a small perturbation. Often, the HS system is used as the reference. Several suggestions have been made for choosing the appropriate HS diameter, d . Below, we list the four HS criteria that in Sec. IV are evaluated with respect to their ability to locate the solid-liquid coexistence line.

In the zero-temperature limit ($T \rightarrow 0$), the WCA pair potential approaches that of a HS⁹⁻¹² system with diameter $d = r_c$, i.e., the system described by

$$v_d(r) = \infty \quad \text{for } r < d \quad (9)$$

and zero otherwise. While this may not be intuitively obvious since the WCA pair potential goes smoothly to zero at the cutoff, it becomes clear when the WCA potential is shown in a log-plot [Fig. 1(b)]. The simplest way of assigning an effective HS diameter to a WCA particle is to use the truncation distance

$$d = r_c. \quad (10)$$

This criterion is exact for $T \rightarrow 0$. At finite temperatures, however, the effective HS diameter will be smaller, and here one needs to make some physical assumptions to improve Eq. (10) and arrive at better approximations. We next list four well-known HS approximations.

1. Boltzmann's hard-sphere criterion

In his 1890 *Lectures on Gas Theory*,⁶⁷ Boltzmann suggested that the effective HS diameter d should be identified with the distance of closest approach when the velocities of two head-on colliding particles are given by their average kinetic energy at far distances. This criterion results in

$$v(d) = k_B T, \quad (11)$$

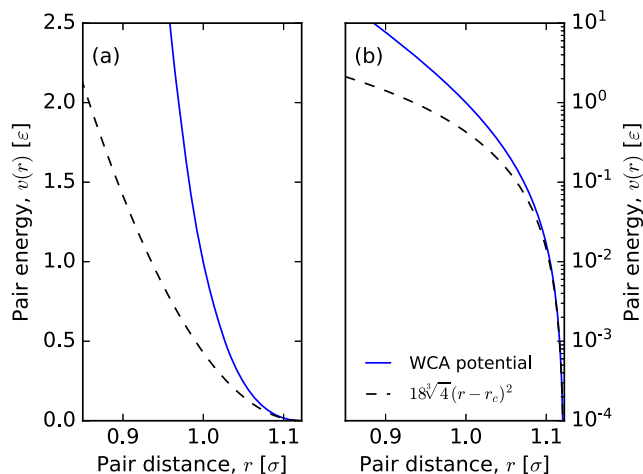


FIG. 1. (a) The solid line shows the WCA pair potential [Eq. (3)], and the dashed line shows the harmonic approximation of Eq. (38). (b) The same pair potential on a logarithmic energy scale, showing a steep slope at low pair energies.

which for the WCA system leads to

$$d = \frac{r_c}{\sqrt[6]{1 + \sqrt{k_B T/\epsilon}}}. \quad (12)$$

Boltzmann's idea, which provides the simplest HS approximation, has been used to estimate the effective HS diameter of the WCA system by a number of authors.^{19–22,24,25}

2. The Andersen-Weeks-Chandler hard-sphere criterion

A more sophisticated HS criterion was suggested in 1971 by Andersen, Weeks, and Chandler (AWC).⁵⁶ Their motivation was to match as well as possible the Helmholtz free energy of the pair potential in question to the associated HS system. The AWC criterion may be summarized as follows: If

$$e(r) = \exp(-v(r)/k_B T) \quad (13)$$

is the pair-potential Boltzmann probability factor, the AWC effective HS diameter d is identified from

$$\int_0^\infty r^2 y_d(r) \Delta e(r) dr = 0 \quad (14)$$

in which $\Delta e(r) = e(r) - e_d(r)$ is the so-called blip function and $y_d(r)$ is the cavity function of the HS fluid. In the Percus-Yevic (PY) approximation, the cavity function is given analytically,^{1,59–62,68,69} which is convenient for applications of Eq. (14). The appearance of the blip function in Eq. (14) effectively limits the AWC integral to values near d . Thus, it is sufficient to consider the zeroth and first shell of $y_d(r)$ to evaluate the AWC integral of Eq. (14) with a high accuracy. We used the following implementation of the cavity function in the determination of the HS diameter d via Eq. (14).⁶⁰ If $s \equiv r/d$,

$$y_d(s) = \begin{cases} c_0 - c_1 s + c_3 s^3 & \text{for } s < 1, \\ H_1(s)/s & \text{for } 1 < s < 2, \end{cases} \quad (15)$$

where

$$H_1(s) = a_1 \exp A(s-1)r + a_2 \exp B(s-1) \cos C(s-1) + a_3 \exp B(s-1) \sin C(s-1). \quad (16)$$

The parameters depend on the packing fraction η [see Eqs. (6) and (15)–(17) in Ref. 60], leading for the coexistence packing fraction $\eta = 0.4909$ (corresponding to the density $0.9375d^{-3}$) to $c_0 = 58.4514$, $c_1 = 67.9928$, $c_3 = 14.3461$, $A = 1.58498$, $B = -3.68494$, $C = 3.85160$, $a_1 = 0.56770$, $a_2 = 4.23705$ and $a_3 = -1.41141$. We evaluated the AWC integral numerically using the Python module SciPy's⁷⁰ implementation of QUADPACK.⁷¹

The pressure of a hard-sphere fluid is given by the value of $y_d(s)$ at the hard-sphere contact distance, $s = 0$. The above theory underestimates the coexistence pressure by only 8%. The PY approximation works best at low densities. Other theoretical approaches^{61,72–78} provide analytical and more accurate expression for the HS radial distribution functions and, in effect, give a better prediction of the pressure. We have not investigated whether the improved theories provide more accurate AWC predictions since they do not provide the needed cavity function as presented. In addition, we have not investigated Lado's refinement⁵⁸ of the AWC theory.

3. The Barker-Henderson hard-sphere criterion

The Barker and Henderson (BH) theory,⁵⁵ which predates the AWC theory, can be viewed as a simplification of the AWC theory.¹ Specifically, it is assumed that r -squared times the cavity-function is a constant, $r^2 y_d = \text{const.}$, implying that Eq. (14) can be written as

$$0 = \int_0^\infty ([1 - e(r)] - [1 - e_d(r)]) dr. \quad (17)$$

Since the integral of $1 - e_d(r)$ is d , one arrives at the following HS criterion:

$$d = \int_0^\infty [1 - e(r)] dr. \quad (18)$$

The $r^2 y_d = \text{const.}$ assumption is reasonable since the blip function limits the integral to values near d where y_d does not change much when the temperature is sufficiently low. As T is lowered, the blip function narrows; thus, the AWC diameter reduces to the BH criterion when $T \rightarrow 0$. Note that the BH criterion depends on temperature but not on density, while the AWC criterion depends on both temperature and density. The BH integral of Eq. (18) is easily evaluated numerically using, e.g., the Python module SciPy's⁷⁰ implementation of QUADPACK.⁷¹

4. Stillinger's hard-sphere criterion

At low temperatures, the integrand of the BH criterion Eq. (18) changes rapidly from nearly unity for $r < d$ to nearly zero for $r > d$. This motivated the HS criterion proposed by Stillinger in 1976.^{40,79,80} He pragmatically identified the HS diameter as the distance at which the pair-potential Boltzmann factor equals one half, i.e.,

$$e(d) = \frac{1}{2}. \quad (19)$$

This was introduced in connection with a study of the Gaussian-core model,⁷⁹ but the same idea can also be applied to the WCA potential leading⁴⁰ to

$$d = \frac{r_c}{\sqrt[6]{1 + \sqrt{k_B T \ln(2)/\epsilon}}}. \quad (20)$$

Note that the functional form of this HS criterion is identical to that of Boltzmann if T is replaced by $T \ln(2)$: The factor 2 comes from Eq. (19); with $e(d) = 1/\exp(1)$, one arrives at Boltzmann's criterion.²⁴

III. NUMERICAL DETERMINATION OF THE PHASE TRANSITION LINE

The interface pinning method^{81–90} is used to compute the solid-liquid chemical potential difference $\Delta\mu$ for isothermal state points at temperatures $0.002\epsilon/k_B$, $0.02\epsilon/k_B$, $0.2\epsilon/k_B$, $2\epsilon/k_B$, and $20\epsilon/k_B$. For a given temperature, we first set up a FCC crystal elongated in the z -direction with the given density and compute the equilibrium pressure in an NVT simulation. From this, a half-crystal/half-fluid configuration is constructed by a high-temperature simulation, where particle positions are only updated for half of the particles (resulting in melting for these particles). This produces a

configuration similar to the one shown in the inset of Fig. 2. We then perform an Np_zT simulation by adding a harmonic bias-field to the potential part of the Hamiltonian,

$$U_{\text{IP}}(\mathbf{R}) = U(\mathbf{R}) + \frac{\kappa}{2}(Q(\mathbf{R}) - a)^2, \quad (21)$$

which forces the system toward configurations with a fluid–crystal interface. Here, κ and a are parameters of the bias-field, and $Q(\mathbf{R})$ is an order parameter that measures crystallinity through long-range order [see Eq. (15) in Ref. 81]. The chemical potential difference between the two phases, $\Delta\mu$, is computed from the average force, $\kappa(Q(\mathbf{R}) - a)$, which the bias field results in on the system [see Eq. (9) in Ref. 81]. This is then repeated for several FCC densities (and thus pressures) near coexistence. As an example, Fig. 2 shows the pressures vs the computed chemical potentials at $2\epsilon/k_B$, considering 11 pressures slightly above $31.7\epsilon/\sigma^3$. The coexistence state point at $\Delta\mu = 0$ is determined by linear regression (compare the solid line in Fig. 2). From this, we find the coexistence pressure $p = 31.8086(66)\epsilon/\sigma^3$, where the number in parentheses gives the statistical error on the last two digits using a 95% confidence interval. Table I reports the thermodynamic coexistence data obtained by the interface-pinning (IP) method and numerical integration of the Clausius–Clapeyron (CC) relation as detailed below.

While the interface-pinning method is accurate and provides specific error estimates, it can be computationally expensive because long simulations are needed to properly represent interface fluctuations, which are usually significantly slower than fluctuations of the bulk solid and fluid.⁸¹ As an alternative, we determine most

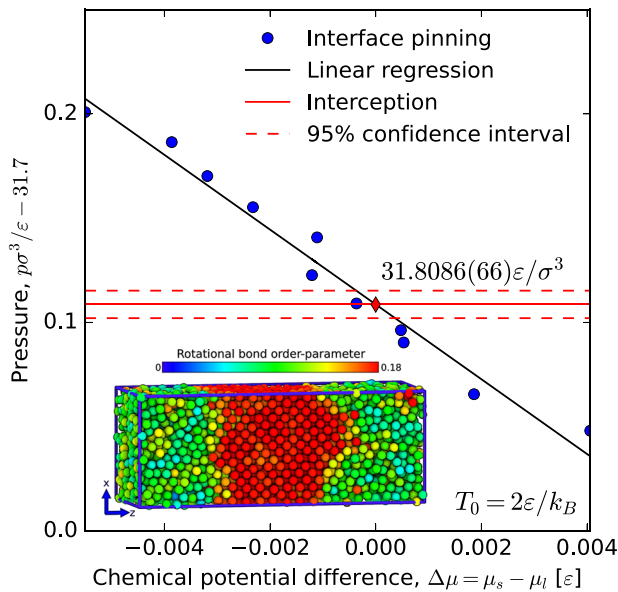


FIG. 2. Determination of the coexistence pressure at the temperature $T_0 = 2\epsilon/k_B$ (red diamond) by means of the interface-pinning method^{81–90} [see Eq. (21)]. The inset shows an interface-pinned configuration where the colors indicate the rotational bond order parameter \bar{q}_4 defined in Ref. 91. With this coloring, crystalline particles are reddish and fluid particles are greenish.

TABLE I. Selected state points on the coexistence line determined by the interface pinning (IP) method and by numerical integration of the Clausius–Clapeyron (CC) relation (all data are available in Zenodo at <http://doi.org/10.5281/zenodo.6505218>). The numbers in parentheses give the statistical uncertainty of the IP data (95% confidence interval).

| T [ϵ/k] | p [ϵ/σ^3] | ρ_l [$1/\sigma^3$] | ρ_s [$1/\sigma^3$] | Method |
|----------------------|-----------------------------|---------------------------|---------------------------|--------|
| 20 | 634.33(14) | 1.784 10(10) | 1.859 34(10) | IP |
| 20 | 633.309 | 1.783 28 | 1.858 50 | CC |
| 2 | 31.808 6(66) | 1.084 41(5) | 1.151 92(6) | IP |
| 2 | 31.753 2 | 1.084 13 | 1.151 63 | CC |
| 0.2 | 2.051 69(33) | 0.800 04(3) | 0.873 56(4) | IP |
| 0.2 | 2.051 18 | 0.799 92 | 0.873 58 | CC |
| 0.02 | 0.174 944(47) | 0.706 38(5) | 0.778 89(6) | IP |
| 0.002 | 0.016 687(3) | 0.677 17(3) | 0.747 91(3) | IP |
| 0.002 | 0.016 680 | 0.677 05 | 0.747 92 | CC |

points on the coexistence line by numerical integration of the Clausius–Clapeyron relation (below s and v are entropy and volume per particle)

$$\frac{dp}{dT} = \frac{\Delta s}{\Delta v}. \quad (22)$$

This is an example of the Gibbs–Duhem integration methods discussed by Kofke,^{92,93} which do not involve slow fluctuations of an interface. The volume difference $\Delta v = v_l - v_s$ and the entropy difference $\Delta s = s_l - s_s = (\Delta u + p\Delta v - \Delta\mu)/T$ can both be evaluated from standard NpT simulations of the two bulk phases at coexistence ($\Delta\mu = 0$).

We use a trapezoidal predictor-corrector method to compute coexistence pressures at the temperatures $T_i = 0.02 \times 10^{(i/24)}$, where i is an integer (compare the solid black line in Fig. 3). Substituting $t = T$ and $y = p$, the first-order differential equation to be solved is rewritten in the standard form as

$$y' = f(t, y), \quad (23)$$

where f is the slope evaluated as $\Delta s/\Delta v$ [Eq. (22)]. Suppose one knows the point (t_i, y_i) on the coexistence line, either from the interface-pinning method or from a previous step of the Clausius–Clapeyron integration, and wishes to compute the next point (t_{i+1}, y_{i+1}) . If $h = t_{i+1} - t_i$, the prediction of the simple Euler algorithm is

$$y_{i+1}^{(0)} = y_i + hf(t_i, y_i). \quad (24)$$

A better estimate is provided by Heun’s method,

$$y_{i+1}^{(1)} = y_i + \frac{h}{2}[f(t_i, y_i) + f(t_i + h, y_{i+1}^{(0)})]. \quad (25)$$

The next estimate in an iterative predictor-corrector approach is

$$y_{i+1}^{(2)} = y_i + \frac{h}{2}[f(t_i, y_i) + f(t_i + h, y_{i+1}^{(1)})] \quad (26)$$

or, in general,

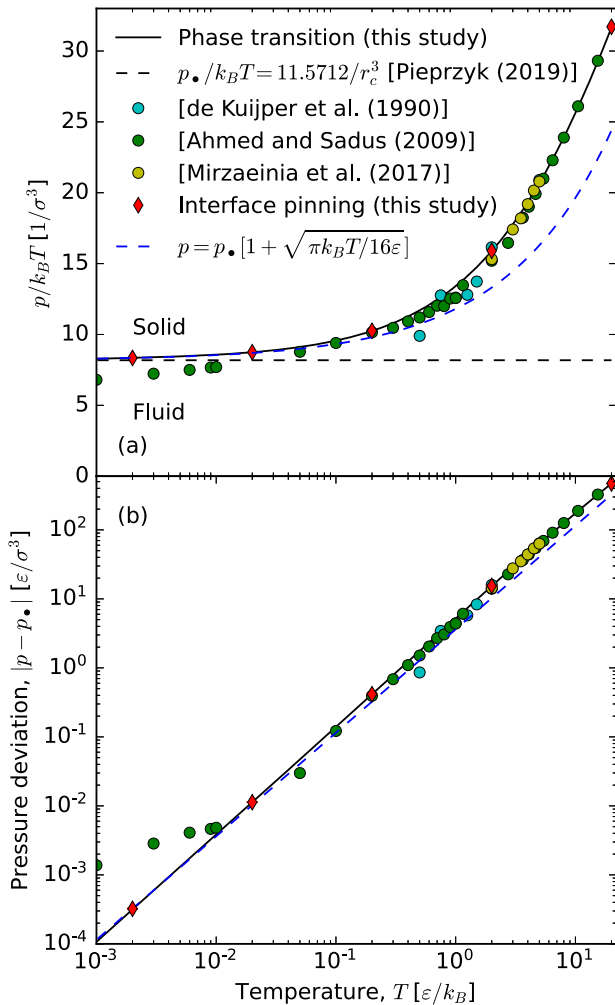


FIG. 3. Coexistence pressure as a function of the temperature. (a) The solid black line shows the reduced coexistence pressure $p/k_B T$ as a function of the temperature (this study). The black dashed line is the $T \rightarrow 0$ HS limit, $p_*/k_B T$, and the colored dots represent literature coexistence pressures.^{42–44} The red diamonds were computed with the interface-pinning method (this study). The blue dashed line shows that at low temperatures, the pressure scales as $T^{3/2}$, as expected from HS theories [inset Eq. (30) into Eq. (46)]. (b) The absolute value of the coexistence pressure in excess of its $T \rightarrow 0$ limit. The red diamonds were computed with the interface-pinning method (this study).

$$y_{i+1}^{k+1} = y_i + \frac{h}{2} [f(t_i, y_i) + f(t_i + h, y_{i+1}^k)]. \quad (27)$$

In the limit of large k 's, this converges to the trapezoidal rule of integration, where forward and backward integrations yield the same result.

Which criterion to use in order to determine when the iterations have converged? To answer this, we note that since the slopes are evaluated from finite NpT simulations, one expects a significant statistical error on the f 's used above. If $\hat{f}(t, y)$ is the theoretical slope, $f(t, y) = \hat{f}(t, y) + e_f$, where e_f is drawn from a

normal distribution with standard deviation σ_f . This error is estimated by dividing NpT simulations into statistically independent blocks.⁹⁴ The error on y_{i+1}^{k+1} is $e_y = h e_f$ and $\sigma_y = |h| \sigma_f$. We terminate the predictor-corrector iteration when

$$|y_{i+1}^{k+1} - y_{i+1}^k| < \sigma_y, \quad (28)$$

since this indicates that changes of y_{i+1} 's are mainly due to the statistical uncertainty on the slopes.

In summary, numerical integration of the Clausius–Clapeyron relation comes with errors from ignoring higher-order terms and

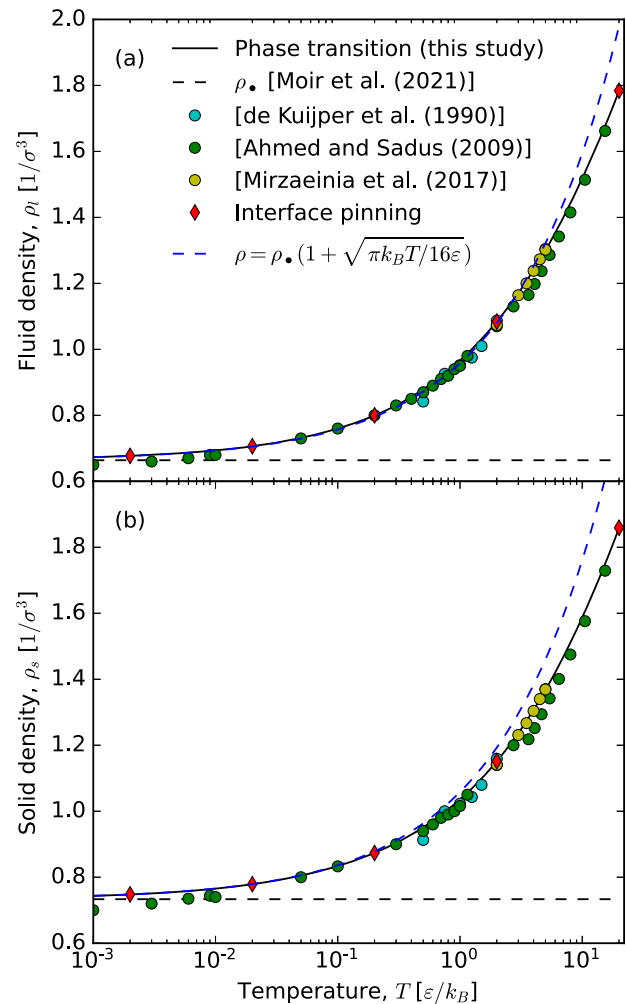


FIG. 4. Fluid density at freezing and solid density at melting as functions of the temperature. (a) The solid black line shows the density of the fluid at coexistence (this study). The dashed line is the $T \rightarrow 0$ limit [see Eq. (47)], and the colored dots are literature data.^{42–44} The red diamonds are densities computed with the interface-pinning method. (b) The solid black line shows the density of the solid at coexistence (this study), the dashed line is the $T \rightarrow 0$ limit, and the colored dots represent literature data.^{42–44} The red diamonds were computed with the interface-pinning method (this study).

from the statistical uncertainty of the slopes. To quantify the overall error of the integration, one can compare to accurate estimates from interface pinning at selected state points. As an example, for $T_{48} = 2\epsilon/k_B$, from the Clausius–Clapeyron integration we estimate the coexistence pressure to be $31.7532\epsilon/\sigma^3$, which should be compared to $31.8086(66)\epsilon/\sigma^3$ for the interface-pinning method (see Table I). The error of the computed phase-transition line is not visible in most figures of this paper, with notable exceptions at low temperatures (error bars are shown in the figures whenever errors are significant).

Figures 3 and 4 show coexistence pressures and densities, respectively, from this study and from the literature.^{42–44} We note that the low-temperature estimates of Ref. 43 are not accurate, whereas the high-temperature estimates of Refs. 42–44 are consistent with our results. As a consistency check, we note that the computed coexistence line reaches the HS limit⁹⁵ when $T \rightarrow 0$ (the dashed lines in Figs. 3 and 4 show the HS limits).

IV. COMPARING THE PREDICTIONS OF DIFFERENT HARD-SPHERE THEORIES

Having accurately located the WCA phase transition, we use this to test the HS theories by comparing their predictions to the low-temperature WCA melting-line data.

A. Coexistence pressure and densities

Starting with the coexistence pressure, we first need coexistence information on the HS system. Fernandez *et al.*⁹⁶ estimated that the HS coexistence pressure is given by $p_d = 11.5727(10)k_B T/d^3$. This value is consistent with

$$p_d = 11.5712(10) k_B T/d^3, \quad (29)$$

computed more recently by Pieprzyk *et al.*,⁹⁵ we use the latter value in this paper. In the zero-temperature limit, the HS diameter of the WCA interaction is $d = r_c$, which gives the coexistence pressure

$$p_\bullet = 8.1821(7) k_B T/\sigma^3. \quad (30)$$

The bullet subscript “•” refers throughout this paper to the HS limit of the WCA model that is approached when $T \rightarrow 0$, i.e., setting $d = r_c$.

The solid black line in Fig. 5(a) shows the coexistence pressure divided by the thermal energy, $p/k_B T$, and the black dashed line shows the $d = r_c$ prediction. The predicted pressure is too low since the effective HS diameter, as mentioned, is smaller than r_c at finite temperatures where particles may overlap. In Fig. 5(a), we also consider other criteria for d 's [by insertions into Eq. (29)]. At $T = 0.02\epsilon/k_B$, the $d = r_c$ criterion underestimates the coexistence pressure by 7%, while the AWC and BH criteria give only a 1% error. Thus, the HS theories give a significant improvement of the predicted coexistence pressure. It is hard to decide from Fig. 5 which theory is best since this depends on the temperature. We return below to the low-temperature limit that provides a definite answer. First, we turn to the HS theories' predictions of the melting- and freezing densities.

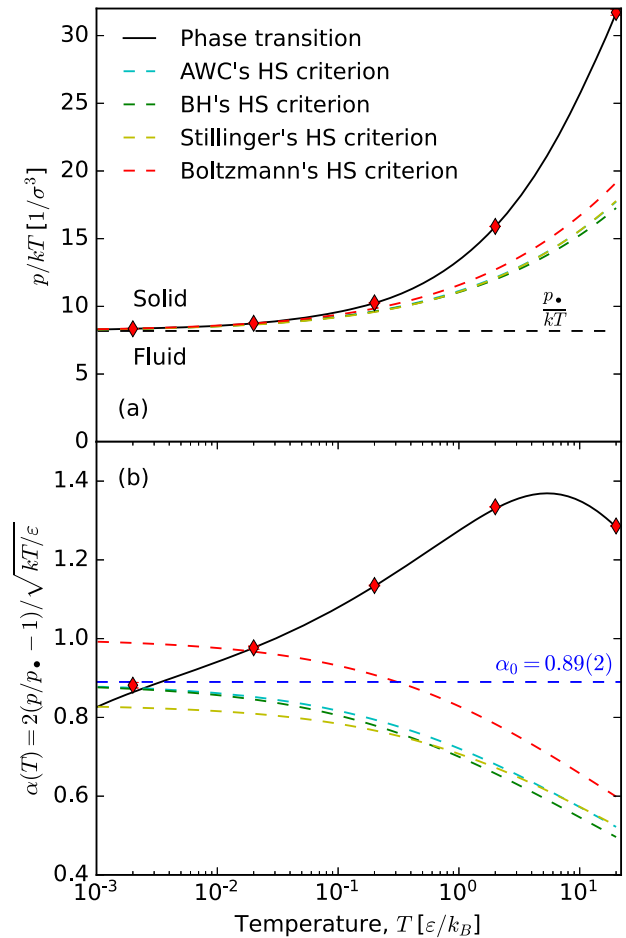


FIG. 5. Melting-line pressure compared to HS predictions. (a) The solid black line shows the reduced coexistence pressure, $p/k_B T$. The dashed lines show predictions of the HS theories [see Eqs. (12), (14), (18), and (20)]. The red diamonds show coexistence pressures computed with the interface-pinning method. (b) $\alpha_p(T) = 2(p/p_\bullet - 1)/\sqrt{k_B T/\epsilon}$ [Eq. (43)] along the computed phase transition line (black solid) and the theoretical predictions also shown in the upper panel (dashed lines). The blue dashed line [$\alpha_0 = 0.89(1)$] is the $T \rightarrow 0$ limit determined from coexistence densities [see Fig. 6(b)]. AWC and BH give accurate predictions in the low-temperature limit. The red diamonds are the results of the interface-pinning method where blue error bars indicate the statistical error. There is a systematic inaccuracy of the Clausius–Clapeyron integration (solid black) at the lowest temperatures.

The HS fluid freezing density was computed recently by Moir, Lue, and Bannerman to the value⁹⁷

$$\rho_d^{(l)} = 0.938\,90(7)/d^3 \quad (31)$$

and the melting density of the solid to

$$\rho_d^{(s)} = 1.037\,15(9)/d^3. \quad (32)$$

In the zero-temperature limit of the WCA system ($d = r_c$), we get

$$\rho_\bullet^{(l)} = 0.663\,90(5)/\sigma^3 \quad (33)$$

and

$$\rho_{\bullet}^{(s)} = 0.733\,37(6)/\sigma^3. \quad (34)$$

When inserting the d 's of the above HS criteria, we get the temperature-dependent density predictions shown in Fig. 6(a) as colored dashed lines.

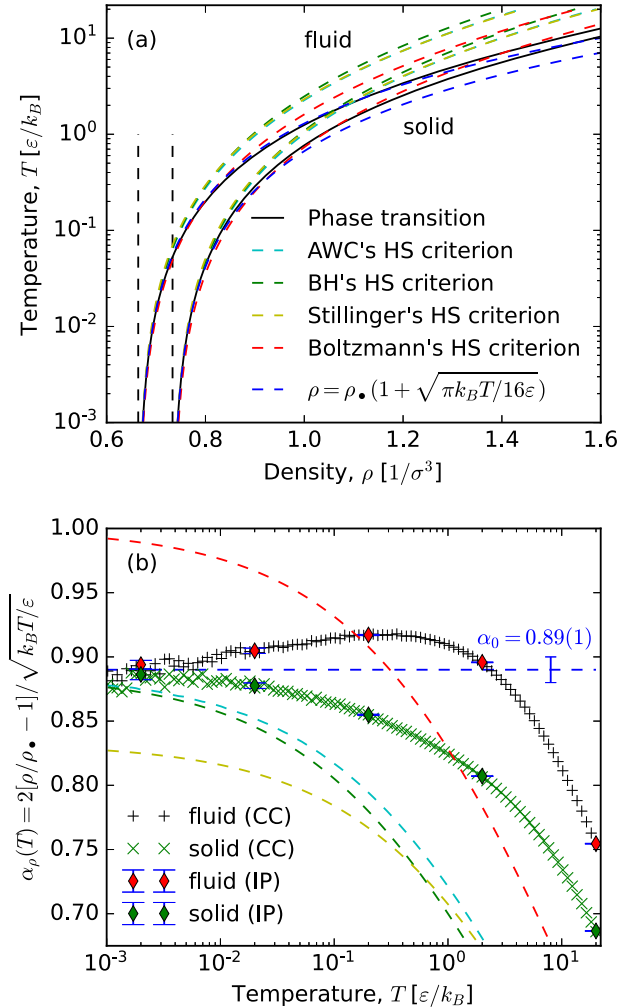


FIG. 6. Density–temperature phase diagram. (a) The solid black lines are the coexistence densities (compare Fig. 4). The vertical black dashed lines mark the $T \rightarrow 0$ HS limits, i.e., the quantities $\rho_{\bullet}^{(l)}$ and $\rho_{\bullet}^{(s)}$. The turquoise, green, yellow, and red dashed curves are predictions of the HS theories, see Eqs. (12), (14), (18), and (20). The two blue dashed lines are the low-temperature fits $\rho_l = \rho_{\bullet}^{(l)} [1 + 0.445\sqrt{k_B T/\epsilon}]$ and $\rho_s = \rho_{\bullet}^{(s)} [1 + 0.445\sqrt{k_B T/\epsilon}]$. (b) The black '+'s show $\alpha_p(T) = 2(\rho/\rho_{\bullet} - 1)/\sqrt{k_B T/\epsilon}$, where the densities ρ and ρ_{\bullet} refer to the fluid. The green 'x's is $\alpha_p(T)$ using the solid densities. Red and green diamonds are densities computed with the interface-pinning method. The blue error bars indicate the 95% confidence interval. We find that the zero-temperature limit gives $\alpha_0 = \lim_{T \rightarrow 0} \alpha(T) = 0.89(1)$. The turquoise, green, yellow, and red dashed curves are predictions of the HS theories. The AWC and BH give the correct low-temperature limit within the statistical accuracy.

B. Analytical treatment of the low-temperature limit

Inspired by the functional form of Stillinger's and Boltzmann's HS criteria [Eqs. (12) and (20)], we write the low-temperature limit of the effective HS diameter as

$$d_{\alpha} = r_c \left(1 - \frac{\alpha_0}{6} \sqrt{k_B T/\epsilon} \right) \quad \text{for } T \rightarrow 0, \quad (35)$$

which implies that

$$d_{\alpha}^{-3} = r_c^{-3} \left(1 + \frac{\alpha_0}{2} \sqrt{k_B T/\epsilon} \right) \quad \text{for } T \rightarrow 0. \quad (36)$$

For the Boltzmann criterion, one has $\alpha_0 = 1$ while Stillinger's criterion gives $\alpha_0 = \sqrt{\ln(2)} \simeq 0.83$.

Since d is the same for the AWC and BH criteria in the $T \rightarrow 0$ limit (see Sec. II B 3), the α_0 's are also identical. To evaluate α_0 , we first note that the BH integral defining the HS diameter [Eq. (18)] can be written as

$$d = r_c - \int_0^{r_c} \exp(-v(r)/k_B T) dr. \quad (37)$$

Since the WCA pair potential is purely repulsive, it reaches its minimum at zero when $r = r_c$. Thus, at low temperatures, the above integral is centered near r_c , i.e., near $x = 0$, where $x = r_c - r$. Keeping the first non-vanishing term in a Taylor expansion, we get

$$v(x) = \frac{1}{2} k_2 x^2 \quad \text{for } T \rightarrow 0 \quad (38)$$

and $x \geq 0$ (distances shorter than r_c) with³⁵

$$k_2 \equiv \left. \frac{d^2 v}{dr^2} \right|_{r_c} = 36\sqrt{4\epsilon/\sigma^2}. \quad (39)$$

(This approximation is shown as a black dashed line in Fig. 1.) Finding d from Eq. (37) involves solving a Gaussian integral in x . Expanding the upper limit of the integral to infinity (which is exact as $T \rightarrow 0$), we find

$$d = r_c - \sqrt{\frac{\pi k_B T}{2k_2}}. \quad (40)$$

By equating $d = d_{\alpha}$ [Eqs. (35) and (40)], we get

$$\alpha_0 = \frac{6}{r_c} \sqrt{\frac{\pi\epsilon}{2k_2}} \quad (41)$$

or $\alpha_0 = \sqrt{\pi}/2 \simeq 0.886\,227$. The theoretical α_0 values are summarized in Table II.

TABLE II. α_0 values.

| From simulations | $\alpha_0 = 0.89(1)$ |
|------------------|--|
| Boltzmann | $\alpha_0 = 1$ |
| AWC and BH | $\alpha_0 = \frac{1}{2}\sqrt{\pi} = 0.886 \dots$ |
| Stillinger | $\alpha_0 = \sqrt{\ln(2)} = 0.833 \dots$ |

To estimate α_0 from the simulations, we insert d_α^{-3} of Eq. (36) into Eq. (29) for the coexistence pressure, leading to

$$p = p_\bullet \left[1 + \frac{\alpha_0}{2} \sqrt{k_B T / \epsilon} \right] \quad \text{for } T \rightarrow 0. \quad (42)$$

Thus, a way to determine α_0 is to define the function [Fig. 5(b)]

$$\alpha_p(T) = \frac{2}{\sqrt{k_B T / \epsilon}} \left[\frac{p(T)}{p_\bullet} - 1 \right], \quad (43)$$

for which we note that $\alpha_0 = \alpha(T)$ for $T \rightarrow 0$. Similarly, for the densities $\rho = \rho_l$ or $\rho = \rho_s$, we get

$$\rho = \rho_\bullet \left[1 + \frac{\alpha_0}{2} \sqrt{k_B T / \epsilon} \right] \quad \text{for } T \rightarrow 0 \quad (44)$$

and define

$$\alpha_\rho(T) = \frac{2}{\sqrt{k_B T / \epsilon}} \left[\frac{\rho(T)}{\rho_\bullet} - 1 \right]. \quad (45)$$

Figure 6(a) shows the temperature dependence of the fluid and solid densities at coexistence (solid lines). These densities yield the $\alpha_\rho(T)$'s shown with black '+'s and green 'x's, respectively, in Fig. 6(b). From the low-temperature points, we estimate $\alpha_0 = 0.89(1)$. The colored dashed lines show the predictions of the HS theories (the $T \rightarrow 0$ limits agree with the values of Table II). We conclude that the AWC and BH theories gives excellent agreement as $T \rightarrow 0$. Figure 5(b) shows $\alpha_p(T)$ computed using the coexistence pressure. In agreement with the results for the $\alpha_\rho(T)$'s, we find that $\alpha_0 = 0.89(1)$ (blue dashed line).

The success of the AWC and BH theories suggests writing the coexistence pressure and densities as follows [inserting $\alpha_0 = \sqrt{\pi}/2$ into Eqs. (42) and (44)]:

$$p = p_\bullet \left[1 + \sqrt{\frac{\pi k_B T}{16\epsilon}} \right] \quad (46)$$

and

$$\rho = \rho_\bullet \left[1 + \sqrt{\frac{\pi k_B T}{16\epsilon}} \right], \quad (47)$$

respectively (see the blue dashed lines of Figs. 3–5). Interestingly, this low-temperature approximation gives better predictions than the neat HS theories—even at high temperatures (with the exception of Boltzmann's criterion near $T \simeq 0.5\epsilon/k_B$). We do not have an explanation for this.

Equations (46) and (47) summarize an important result of this paper, providing an analytical HS approximation for the low-temperature freezing of the WCA fluid. This can be generalized to any other purely repulsive pair-potential $v(r)$ that is truncated smoothly at $r = r_c$ by the following steps:

1. Compute k_2 using Eq. (39).
2. Derive α_0 within the BH theory by inserting k_2 into Eq. (41).
3. Low-temperature predictions for the coexistence pressure and densities are then provided by inserting α_0 into Eqs. (42) and (44), respectively.

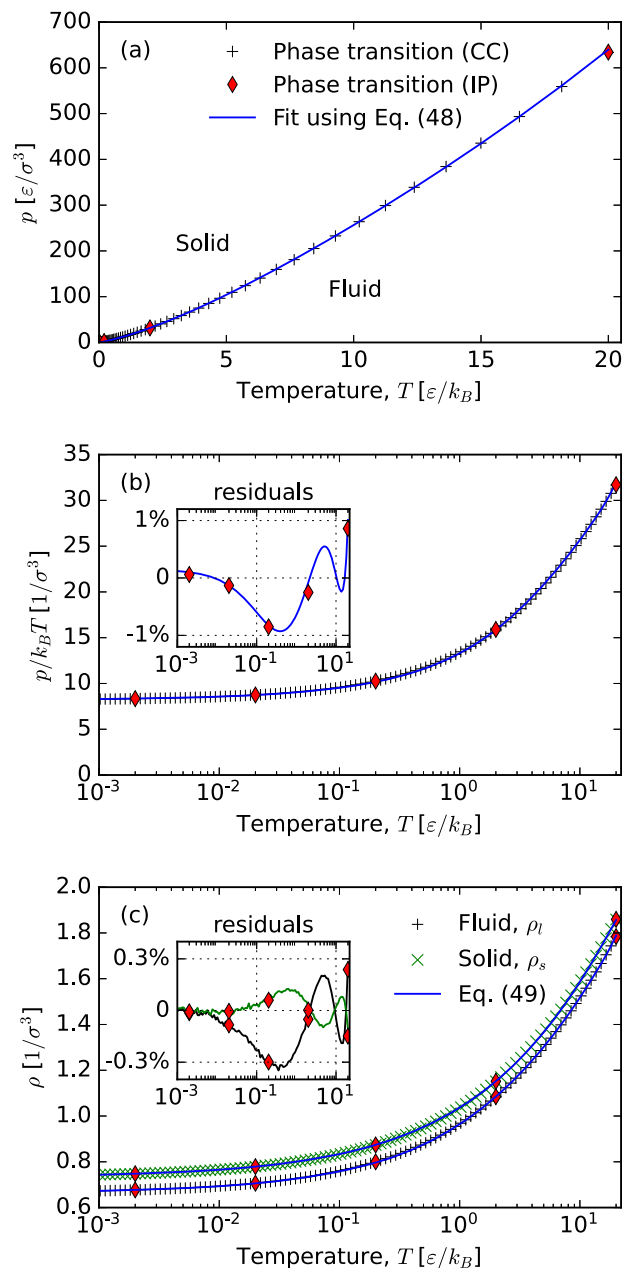


FIG. 7. (a) Empirical fit [Eq. (48) (blue dashed line)] to the phase transition pressure (+). The red diamonds show the phase transition pressure computed with the interface pinning method. (b) Empirical fit [Eq. (48)] to the reduced pressure, p/T . The inset shows the residuals in percent. (c) Empirical fit [Eq. (49)] to the freezing density of the fluid (ρ_l) and the melting density of the solid (ρ_s).

C. Empirical fit to the coexistence line

We have provided a theory for low temperatures. To provide a practical description of the coexistence line that includes high temperatures, we continue the power series in $\tau = \sqrt{k_B T / \epsilon}$ by writing the coexistence pressure as

$$p(T) = p_{\bullet} \left[1 + \sqrt{\frac{\pi}{16}} \tau + \tilde{a}_2 \tau^2 + \tilde{a}_3 \tau^3 + \tilde{a}_4 \tau^4 \right]. \quad (48)$$

The parameters $\tilde{a}_2 = 0.2619$, $\tilde{a}_3 = -0.0871$, and $\tilde{a}_4 = 0.0087$ are determined by non-linear least squares to fit to the reduced pressure, p/T [see Eq. (30) for p_{\bullet}]. The accuracy of the fit is within 1% for the investigated temperatures [see Figs. 7(a) and 7(b)]. Similar for the coexistence densities, we define

$$\rho(T) = \rho_{\bullet} \left[1 + \sqrt{\frac{\pi}{16}} \tau + \tilde{a}_2 \tau^2 + \tilde{a}_3 \tau^3 + \tilde{a}_4 \tau^4 \right]. \quad (49)$$

A non-linear least squares fit to the freezing density of the liquid (ρ_l) yields $\tilde{a}_2 = 0.0240$, $\tilde{a}_3 = -0.0178$, and $\tilde{a}_4 = 0.00206$. A fit to the melting density of the solid (ρ_s) yields $\tilde{a}_2 = -0.03336$, $\tilde{a}_3 = 0.00447$, and $\tilde{a}_4 = -0.000457$ [see Eqs. (33) and (34) for $\rho_{\bullet} = \rho_{\bullet}^{(l)}$ and $\rho_{\bullet} = \rho_{\bullet}^{(s)}$, respectively]. The accuracy of the fits is within 0.3% and 0.15% for the liquid and solid densities, respectively. The fits to the densities are shown in Fig. 7(c).

V. OUTLOOK

We have shown that HS theories give excellent predictions of the WCA melting line at low temperatures, in particular, for the AWC and BH approximations. At higher temperatures, the HS theories are less accurate. This is not surprising because the WCA model only resembles a HS system at low temperatures. How to predict the WCA melting-line pressures and coexistence densities at high temperatures? One possibility is to generalize the low-temperature HS approximation by considering the lines of constant excess entropy S_{ex} (the entropy in excess of the ideal gas entropy at the same density and temperature, a negative quantity that in some textbooks⁹⁸ is referred to as the residual entropy). For the HS system, these lines are determined entirely by the density, i.e., they are vertical in the density–temperature phase diagram. In Ref. 35, it was shown that the WCA system’s structure and dynamics are near-invariant along the lines of constant excess entropy, which are referred to as isomorphs.^{99,100} An isomorph can be computed by

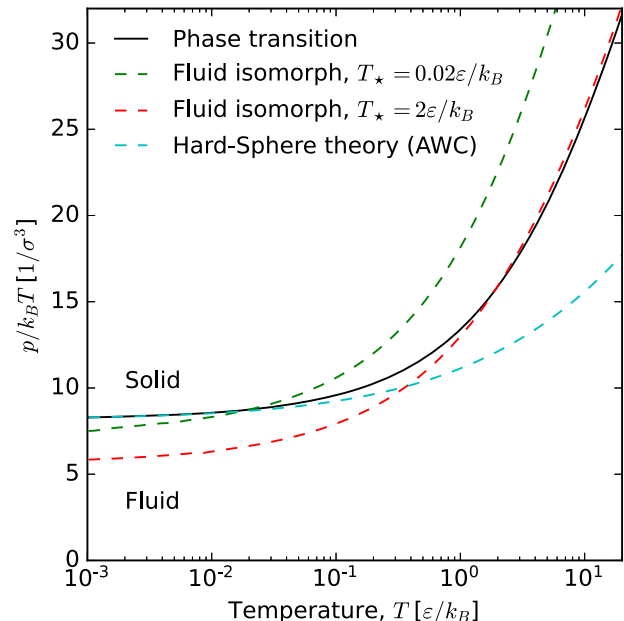


FIG. 8. The solid black line shows the reduced coexistence pressure $p/k_B T$ as a function of the temperature. The red and green dashed lines are isomorphs of the fluid, i.e., lines along which the excess entropy is constant. By construction, the isomorphs touch the phase-transition line at $T_* = 0.02\epsilon/k_B$ and $T_* = 2\epsilon/k_B$, respectively. The turquoise dashed line is the prediction of the AWC theory.

numerical integration in the $\ln T - \ln \rho$ plane [e.g., using the fourth-order Runge–Kutta method (RK4)³⁵] for which the required slope is $f = 1/\gamma$, where^{99,101,102}

$$\gamma \equiv \left(\frac{\partial \ln T}{\partial \ln \rho} \right)_{S_{\text{ex}}}. \quad (50)$$

The “density-scaling exponent” γ may be computed from virial and potential-energy fluctuations in the NVT ensemble via the statistical-mechanical identity $\gamma = \langle \Delta W \Delta U \rangle / \langle (\Delta U)^2 \rangle$.⁹⁹ Figure 8 shows the reduced pressure $p/k_B T$ of two fluid isomorphs that

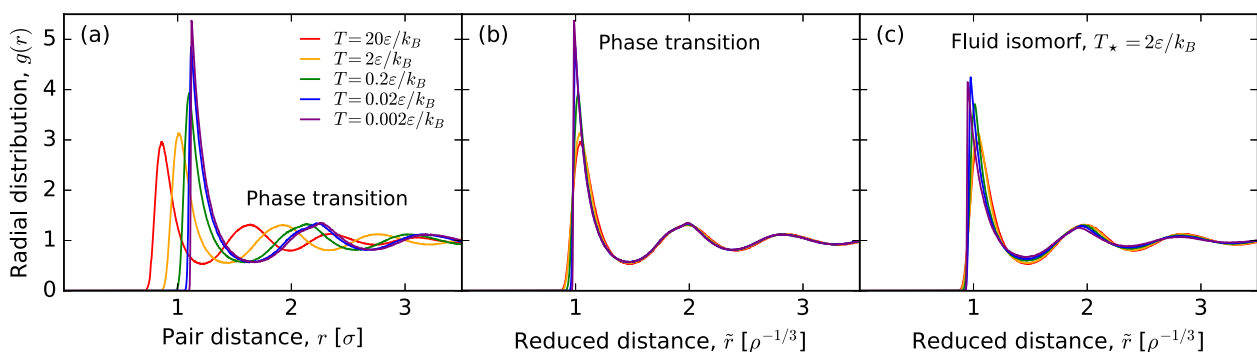


FIG. 9. (a) The radial distribution function $g(r)$ of the fluid at coexistence. (b) The radial distribution function as a function of the reduced distance $\tilde{r} = r\sqrt[3]{\rho}$ for the fluid at coexistence. (c) The radial distribution as a function of the reduced distance $\tilde{r} = r\sqrt[3]{\rho}$ for a fluid isomorph that touches the coexistence line at $T_* = 2\epsilon/k_B$.

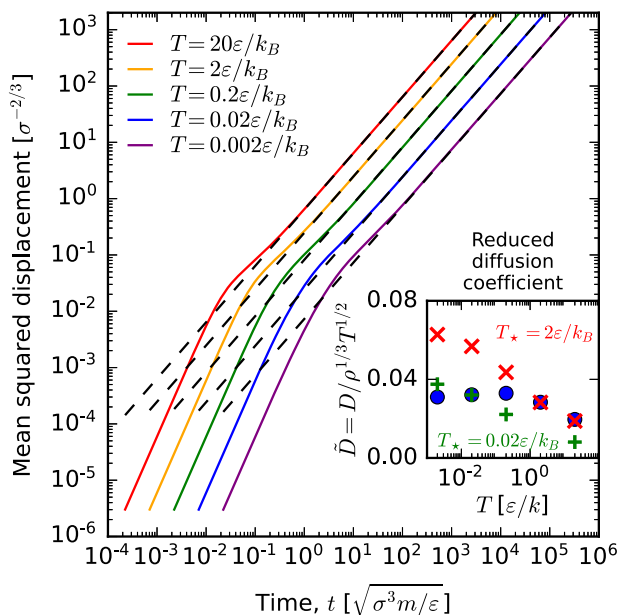


FIG. 10. The solid lines show the mean-square displacement $\langle |r(t) - r(0)|^2 \rangle$ for selected state points along the coexistence line (see Table I). The dashed lines are long-time fits to $\langle |r(t) - r(0)|^2 \rangle = 6Dt$, where D is the diffusion coefficient. The dots in the inset show the reduced diffusion coefficient $\tilde{D} = D\rho^{1/3}T^{1/2}$. The red 'x's and green '+'s are the reduced diffusion coefficient for state points along the isomorphs with $T_* = 2\varepsilon/k_B$ and $T_* = 0.02\varepsilon/k_B$, respectively.

overlap with the coexistence line at $T_* = 0.02\varepsilon/k_B$ and $T_* = 2\varepsilon/k_B$, respectively (dashed green and red lines). For comparison, the turquoise dashed line shows the prediction of the reduced coexistence pressure of the AWC theory. For the entire temperature span, the isomorphs give predictions with an overall accuracy comparable to that of the best HS approximation (AWC).

Figures 9 and 10 show the structure and dynamics along the melting line and the fluid isomorph in reduced units.⁹⁹ The physics is more invariant along the coexistence lines than along the isomorph, which is in contrast to previous findings for the LJ system where the opposite applies.¹⁰³ We note, however, that isomorphs only follow the coexistence lines to a first approximation. For the LJ system, accurate predictions for the thermodynamics of freezing and melting are arrived at within the isomorph-theoretical perturbation framework proposed in Ref. 103—we plan to apply the same method to the WCA system.

ACKNOWLEDGMENTS

This work was supported by the VILLUM Foundation's Matter Grant (No. 16515).

AUTHOR DECLARATIONS

Conflict of Interest

The authors have no conflicts to disclose.

Author Contributions

Eman Attia: Data curation (equal); Investigation (equal). **Jeppe C. Dyre:** Conceptualization (supporting); Formal analysis (supporting); Funding acquisition (lead); Supervision (equal); Writing – original draft (supporting); Writing – review & editing (supporting). **Ulf R. Pedersen:** Conceptualization (lead); Data curation (lead); Formal analysis (equal); Investigation (lead); Software (lead); Supervision (equal); Validation (lead); Visualization (lead); Writing – original draft (lead); Writing – review & editing (lead).

DATA AVAILABILITY

The data that support the findings of this study are openly available in Zenodo at <http://doi.org/10.5281/zenodo.6505217>, reference number 6505217.

REFERENCES

- J.-P. Hansen and I. R. McDonald, *Theory of Simple Liquids: With Applications to Soft Matter*, 4th ed. (Academic, New York, 2013).
- W. G. Hoover, S. G. Gray, and K. W. Johnson, "Thermodynamic properties of the fluid and solid phases for inverse power potentials," *J. Chem. Phys.* **55**, 1128–1136 (1971).
- W. G. Hoover, D. A. Young, and R. Grover, "Statistical mechanics of phase diagrams. I. Inverse power potentials and the close-packed to body-packed cubic transition," *J. Chem. Phys.* **56**, 2207–2210 (1972).
- D. M. Heyes and A. C. Brańka, "Physical properties of soft repulsive particle fluids," *Phys. Chem. Chem. Phys.* **9**, 5570–5575 (2007).
- A. C. Branka and D. M. Heyes, "Pair correlation function of soft-sphere fluids," *J. Chem. Phys.* **134**, 064115 (2011).
- A. K. Bacher, T. B. Schröder, and J. C. Dyre, "The EXP pair-potential system. I. Fluid phase isotherms, isochores, and quasiuniversality," *J. Chem. Phys.* **149**, 114501 (2019).
- A. K. Bacher, T. B. Schröder, and J. C. Dyre, "The EXP pair-potential system. II. Fluid phase isomorphs," *J. Chem. Phys.* **149**, 114502 (2018).
- U. R. Pedersen, A. K. Bacher, T. B. Schröder, and J. C. Dyre, "The EXP pair-potential system. III. Thermodynamic phase diagram," *J. Chem. Phys.* **150**, 174501 (2019).
- B. J. Alder and T. E. Wainwright, "Phase transition for a hard sphere system," *J. Chem. Phys.* **27**, 1208–1209 (1957).
- W. W. Wood and J. D. Jacobson, "Preliminary results from a recalculation of the Monte Carlo equation of state of hard spheres," *J. Chem. Phys.* **27**, 1207–1208 (1957).
- B. J. Alder and T. E. Wainwright, "Studies in molecular dynamics. I. General method," *J. Chem. Phys.* **31**, 459–466 (1959).
- B. J. Alder and T. E. Wainwright, "Studies in molecular dynamics. II. Behavior of a small number of elastic spheres," *J. Chem. Phys.* **33**, 1439–1451 (1960).
- J. O. Hirschfelder, C. F. Curtiss, and R. B. Bird, *Molecular Theory of Gases and Liquids* (John Wiley & Sons, New York, 1954).
- J. D. Bernal, "The Bakerian lecture, 1962. The structure of liquids," *Proc. R. Soc. London, Ser. A* **280**, 299–322 (1964).
- B. Widom, "Intermolecular forces and the nature of the liquid state," *Science* **157**, 375–382 (1967).
- J. A. Barker and D. Henderson, "What is 'liquid'? Understanding the states of matter," *Rev. Mod. Phys.* **48**, 587–671 (1976).
- J. D. Weeks, D. Chandler, and H. C. Andersen, "Role of repulsive forces in determining the equilibrium structure of simple liquids," *J. Chem. Phys.* **54**, 5237–5247 (1971).
- D. Chandler, J. D. Weeks, and H. C. Andersen, "Van der Waals picture of liquids, solids, and phase transformations," *Science* **220**, 787–794 (1983).
- F. C. Andrews, "A simple approach to the equilibrium statistical mechanics of two-dimensional fluids," *J. Chem. Phys.* **64**, 1941–1947 (1976).

- ²⁰R. J. Speedy, F. X. Prielmeier, T. Vardag, E. W. Lang, and H.-D. Lüdemann, "Diffusion in simple fluids," *Mol. Phys.* **66**, 577–590 (1989).
- ²¹D. Ben-Amotz and D. R. Herschbach, "Estimation of effective diameters for molecular fluids," *J. Phys. Chem.* **94**, 1038–1047 (1990).
- ²²S. Hess, M. Kröger, and H. Voigt, "Thermomechanical properties of the WCA–Lennard-Jones model system in its fluid and solid states," *Physica A* **250**, 58–82 (1998).
- ²³D. Ben-Amotz and G. Stell, "Hard sphere perturbation theory for fluids with soft-repulsive-core potentials," *J. Chem. Phys.* **120**, 4844–4851 (2004).
- ²⁴D. Ben-Amotz and G. Stell, "Reformulation of Weeks–Chandler–Andersen perturbation theory directly in terms of a hard-sphere reference system," *J. Phys. Chem. B* **108**, 6877–6882 (2004).
- ²⁵D. M. Heyes and H. Okumura, "Equation of state and structural properties of the Weeks–Chandler–Andersen fluid," *J. Chem. Phys.* **124**, 164507 (2006).
- ²⁶L. Berthier and G. Tarjus, "Nonperturbative effect of attractive forces in viscous liquids," *Phys. Rev. Lett.* **103**, 170601 (2009).
- ²⁷U. R. Pedersen, T. B. Schröder, and J. C. Dyre, "Repulsive reference potential reproducing the dynamics of a liquid with attractions," *Phys. Rev. Lett.* **105**, 157801 (2010).
- ²⁸L. Berthier and G. Tarjus, "The role of attractive forces in viscous liquids," *J. Chem. Phys.* **134**, 214503 (2011).
- ²⁹S. A. Khrapak, M. Chaudhuri, and G. E. Morfill, "Communication: Universality of the melting curves for a wide range of interaction potentials," *J. Chem. Phys.* **134**, 241101 (2011).
- ³⁰L. Böhling, A. A. Veldhorst, T. S. Ingebrigtsen, N. P. Bailey, J. S. Hansen, S. Toxvaerd, T. B. Schröder, and J. C. Dyre, "Do the repulsive and attractive pair forces play separate roles for the physics of liquids?," *J. Phys.: Condens. Matter* **25**, 032101 (2012).
- ³¹Z. E. Dell and K. S. Schweizer, "Microscopic theory for the role of attractive forces in the dynamics of supercooled liquids," *Phys. Rev. Lett.* **115**, 205702 (2015).
- ³²L.-C. Valdès, J. Gerges, T. Mizuguchi, and F. Affouard, "Crystallization tendencies of modelled Lennard-Jones liquids with different attractions," *J. Chem. Phys.* **148**, 014501 (2018).
- ³³J. Chatteraj and M. P. Ciamarra, "Role of attractive forces in the relaxation dynamics of supercooled liquids," *Phys. Rev. Lett.* **124**, 028001 (2020).
- ³⁴Y. Zhou, B. Mei, and K. S. Schweizer, "Integral equation theory of thermodynamics, pair structure, and growing static length scale in metastable hard sphere and Weeks–Chandler–Andersen fluids," *Phys. Rev. E* **101**, 042121 (2020).
- ³⁵E. Attia, J. C. Dyre, and U. R. Pedersen, "Extreme case of density scaling: The Weeks–Chandler–Andersen system at low temperatures," *Phys. Rev. E* **103**, 062140 (2021).
- ³⁶S. S. Khali, D. Chakraborty, and D. Chaudhuri, "Two-step melting of the Weeks–Chandler–Anderson system in two dimensions," *Soft Matter* **17**, 3473–3485 (2021).
- ³⁷A. Banerjee and D. J. Wales, "Energy landscapes for a modified repulsive Weeks–Chandler–Andersen potential," *J. Phys.: Condens. Matter* **34**, 034004 (2021).
- ³⁸S. Toxvaerd, "Role of the attractive forces in a supercooled liquid," *Phys. Rev. E* **103**, 022611 (2021).
- ³⁹A. Singh and Y. Singh, "How attractive and repulsive interactions affect structure ordering and dynamics of glass-forming liquids," *Phys. Rev. E* **103**, 052105 (2021).
- ⁴⁰D. M. Heyes, S. Pieprzyk, and A. C. Brańka, "Application of cell models to the melting and sublimation lines of the Lennard-Jones and related potential systems," *Phys. Rev. E* **104**, 044119 (2021).
- ⁴¹Y. Zhou, B. Mei, and K. S. Schweizer, "Activated relaxation in supercooled monodisperse atomic and polymeric WCA fluids: Simulation and ECNLE theory," *J. Chem. Phys.* **156**, 114901 (2022).
- ⁴²A. de Kuijper, J. A. Schouten, and J. P. J. Michels, "The melting line of the Weeks–Chandler–Anderson Lennard-Jones reference system," *J. Chem. Phys.* **93**, 3515–3519 (1990).
- ⁴³A. Ahmed and R. J. Sadus, "Phase diagram of the Weeks–Chandler–Andersen potential from very low to high temperatures and pressures," *Phys. Rev. E* **80**, 061101 (2009).
- ⁴⁴A. Mirzaeinia, F. Feyzi, and S. M. Hashemianzadeh, "Equation of state and Helmholtz free energy for the atomic system of the repulsive Lennard-Jones particles," *J. Chem. Phys.* **147**, 214503 (2017).
- ⁴⁵J. E. Lennard-Jones, "On the determination of molecular fields.—I. From the variation of the viscosity of a gas with temperature," *Proc. R. Soc. London, Ser. A* **106**, 441–462 (1924).
- ⁴⁶J. E. Lennard-Jones, "On the determination of molecular fields.—II. From the equation of state of a gas," *Proc. R. Soc. London, Ser. A* **106**, 463–477 (1924).
- ⁴⁷N. Bailey, T. Ingebrigtsen, J. S. Hansen, A. Veldhorst, L. Böhling, C. Lemarchand, A. Olsen, A. Bacher, L. Costigliola, U. R. Pedersen, H. Larsen, J. C. Dyre, and T. Schröder, "RUMD: A general purpose molecular dynamics package optimized to utilize GPU hardware down to a few thousand particles," *SciPost Phys.* **3**, 038 (2017).
- ⁴⁸D. Frenkel and B. Smit, *Understanding Molecular Simulation: From Algorithms to Applications*, 2nd ed. (Academic Press, San Diego, 2002).
- ⁴⁹N. Grønbech-Jensen, "Complete set of stochastic Verlet-type thermostats for correct Langevin simulations," *Mol. Phys.* **118**, e1662506 (2019).
- ⁵⁰N. Grønbech-Jensen and O. Farago, "Constant pressure and temperature discrete-time Langevin molecular dynamics," *J. Chem. Phys.* **141**, 194108 (2014).
- ⁵¹N. Grønbech-Jensen, N. R. Hayre, and O. Farago, "Application of the G-JF discrete-time thermostat for fast and accurate molecular simulations," *Comput. Phys. Commun.* **185**, 524–527 (2014).
- ⁵²R. W. Zwanzig, "High-temperature equation of state by a perturbation method. I. Nonpolar gases," *J. Chem. Phys.* **22**, 1420–1426 (1954).
- ⁵³J. S. Rowlinson, "An equation of state of gases at high temperatures and densities," *Mol. Phys.* **7**, 349–361 (1964).
- ⁵⁴H. L. Frisch, J. L. Katz, E. Praetgaard, and J. L. Lebowitz, "High-temperature equation of state—Argon," *J. Phys. Chem.* **70**, 2016–2020 (1966).
- ⁵⁵J. A. Barker and D. Henderson, "Perturbation theory and equation of state for fluids. II. A successful theory of liquids," *J. Chem. Phys.* **47**, 4714–4721 (1967).
- ⁵⁶H. C. Andersen, J. D. Weeks, and D. Chandler, "Relationship between the hard-sphere fluid and fluids with realistic repulsive forces," *Phys. Rev. A* **4**, 1597–1607 (1971).
- ⁵⁷L. Verlet and J.-J. Weis, "Perturbation theory for the thermodynamic properties of simple liquids," *Mol. Phys.* **24**, 1013–1024 (1972).
- ⁵⁸F. Lado, "Choosing the reference system for liquid state perturbation theory," *Mol. Phys.* **52**, 871–876 (1984).
- ⁵⁹G. Kahl, "Analytic representation for the pair-correlation function of a hard-sphere Yukawa system," *Mol. Phys.* **67**, 879–889 (1989).
- ⁶⁰J. Chang and S. I. Sandler, "A real function representation for the structure of the hard-sphere fluid," *Mol. Phys.* **81**, 735–744 (1994).
- ⁶¹A. Trokhymchuk, I. Nezbeda, J. Jirsák, and D. Henderson, "Hard-sphere radial distribution function again," *J. Chem. Phys.* **123**, 024501 (2005).
- ⁶²D. Henderson, "Analytic methods for the Percus–Yevick hard sphere correlation functions," *Condens. Matter Phys.* **12**, 127–135 (2009).
- ⁶³J. C. Dyre, "'Simple liquids' quasiuniversality and the hard-sphere paradigm," *J. Phys.: Condens. Matter* **28**, 323001 (2016).
- ⁶⁴J. R. Solana, *Perturbation Theories for the Thermodynamic Properties of Fluids and Solids* (CRC Press, London, England, 2019).
- ⁶⁵B. P. Akhouri and J. R. Solana, "On the choice of the effective diameter in the high-temperature expansion for the Lennard-Jones fluid," *Mol. Phys.* **120**, e2028918 (2022).
- ⁶⁶T. van Westen, M. Hammer, B. Hafskjold, A. Aasen, J. Gross, and Ø. Wilhelmsen, "Perturbation theories for fluids with short-ranged attractive forces: A case study of the Lennard-Jones spline fluid," *J. Chem. Phys.* **156**, 104504 (2022).
- ⁶⁷L. Boltzmann, *Lectures on Gas Theory* (Dover Publications, 1864).
- ⁶⁸M. S. Wertheim, "Exact solution of the Percus–Yevick integral equation for hard spheres," *Phys. Rev. Lett.* **10**, 321–323 (1963).
- ⁶⁹W. R. Smith, D. J. Henderson, P. J. Leonard, J. A. Barker, and E. W. Grundke, "Fortran codes for the correlation functions of hard sphere fluids," *Mol. Phys.* **106**, 3–7 (2008).
- ⁷⁰P. Virtanen et al., "SciPy 1.0: Fundamental algorithms for scientific computing in Python," *Nat. Methods* **17**, 261–272 (2020).

- ⁷¹R. Piessens, E. De Doncker-Kapenga, C. Uberhuber, and D. K. Kahaner, *Quadrack*, Springer Series in Computational Mathematics (Springer, Berlin, Germany, 1983).
- ⁷²L. Verlet, "Integral equations for classical fluids. I. The hard sphere case," *Mol. Phys.* **41**, 183–190 (1980).
- ⁷³L. Verlet, "Integral equations for classical fluids. II. Hard spheres again," *Mol. Phys.* **42**, 1291–1302 (1981).
- ⁷⁴G. A. Martynov and G. N. Sarkisov, "Exact equations and the theory of liquids. V," *Mol. Phys.* **49**, 1495–1504 (1983).
- ⁷⁵S. B. Yuste and A. Santos, "Radial distribution function for hard spheres," *Phys. Rev. A* **43**, 5418–5423 (1991).
- ⁷⁶Y. Tang and B. C. Y. Lu, "Improved expressions for the radial distribution function of hard spheres," *J. Chem. Phys.* **103**, 7463–7470 (1995).
- ⁷⁷*Theory and Simulation of Hard-Sphere Fluids and Related Systems*, edited by A. Mulero (Springer, Berlin, Heidelberg, 2008).
- ⁷⁸A. Santos, S. B. Yuste, and M. López de Haro, "Structural and thermodynamic properties of hard-sphere fluids," *J. Chem. Phys.* **153**, 120901 (2020).
- ⁷⁹F. H. Stillinger, "Phase transitions in the Gaussian core system," *J. Chem. Phys.* **65**, 3968–3974 (1976).
- ⁸⁰C. N. Likos, "Effective interactions in soft condensed matter physics," *Phys. Rep.* **348**, 267–439 (2001).
- ⁸¹U. R. Pedersen, "Direct calculation of the solid-liquid Gibbs free energy difference in a single equilibrium simulation," *J. Chem. Phys.* **139**, 104102 (2013).
- ⁸²U. R. Pedersen, F. Hummel, G. Kresse, G. Kahl, and C. Dellago, "Computing Gibbs free energy differences by interface pinning," *Phys. Rev. B* **88**, 094101 (2013).
- ⁸³V. Thapar and F. A. Escobedo, "Extensions of the interfacial pinning method and application to hard core systems," *J. Chem. Phys.* **141**, 124117 (2014).
- ⁸⁴U. R. Pedersen, F. Hummel, and C. Dellago, "Computing the crystal growth rate by the interface pinning method," *J. Chem. Phys.* **142**, 044104 (2015).
- ⁸⁵B. Cheng, E. A. Engel, J. Behler, C. Dellago, and M. Ceriotti, "Ab initio thermodynamics of liquid and solid water," *Proc. Natl. Acad. Sci. U. S. A.* **116**, 1110–1115 (2019).
- ⁸⁶R. S. Newman, S. Nola, J. Dshemuchadse, and S. C. Glotzer, "Shape-controlled crystallisation pathways in dense fluids of *ccp*-forming hard polyhedra," *Mol. Phys.* **117**, 3819–3826 (2019).
- ⁸⁷K. G. Steenbergen, E. Pahl, and P. Schwerdtfeger, "Accurate, large-scale density functional melting of Hg: Relativistic effects decrease melting temperature by 160 K," *J. Phys. Chem. Lett.* **8**, 1407–1412 (2017).
- ⁸⁸A. K. Sharma and F. A. Escobedo, "Nucleus-size pinning for determination of nucleation free-energy barriers and nucleus geometry," *J. Chem. Phys.* **148**, 184104 (2018).
- ⁸⁹Y. Zou, S. Xiang, and C. Dai, "Investigation on the efficiency and accuracy of methods for calculating melting temperature by molecular dynamics simulation," *Comput. Mater. Sci.* **171**, 109156 (2020).
- ⁹⁰L.-F. Zhu, J. Janssen, S. Ishibashi, F. Körmann, B. Grabowski, and J. Neugebauer, "A fully automated approach to calculate the melting temperature of elemental crystals," *Comput. Mater. Sci.* **187**, 110065 (2021).
- ⁹¹W. Lechner and C. Dellago, "Accurate determination of crystal structures based on averaged local bond order parameters," *J. Chem. Phys.* **129**, 114707 (2008).
- ⁹²D. A. Kofke, "Gibbs-Duhem integration: A new method for direct evaluation of phase coexistence by molecular simulation," *Mol. Phys.* **78**, 1331–1336 (1993).
- ⁹³D. A. Kofke, "Direct evaluation of phase coexistence by molecular simulation via integration along the saturation line," *J. Chem. Phys.* **98**, 4149–4162 (1993).
- ⁹⁴H. Flyvbjerg and H. G. Petersen, "Error estimates on averages of correlated data," *J. Chem. Phys.* **91**, 461–466 (1989).
- ⁹⁵S. Pieprzyk, M. N. Bannerman, A. C. Brańka, M. Chudak, and D. M. Heyes, "Thermodynamic and dynamical properties of the hard sphere system revisited by molecular dynamics simulation," *Phys. Chem. Chem. Phys.* **21**, 6886–6899 (2019).
- ⁹⁶L. A. Fernández, V. Martín-Mayor, B. Seoane, and P. Verrocchio, "Equilibrium fluid-solid coexistence of hard spheres," *Phys. Rev. Lett.* **108**, 165701 (2012).
- ⁹⁷C. Moir, L. Lue, and M. N. Bannerman, "Tethered-particle model: The calculation of free energies for hard-sphere systems," *J. Chem. Phys.* **155**, 064504 (2021).
- ⁹⁸I. Prigogine and R. Defay, *Chemical Thermodynamics* (Prentice Hall Press, 1954).
- ⁹⁹N. Gnan, T. B. Schröder, U. R. Pedersen, N. P. Bailey, and J. C. Dyre, "Pressure-energy correlations in liquids. IV. 'Isomorphs' in liquid phase diagrams," *J. Chem. Phys.* **131**, 234504 (2009).
- ¹⁰⁰T. B. Schröder and J. C. Dyre, "Simplicity of condensed matter at its core: Generic definition of a Roskilde-simple system," *J. Chem. Phys.* **141**, 204502 (2014).
- ¹⁰¹J. C. Dyre, "Hidden scale invariance in condensed matter," *J. Phys. Chem. B* **118**, 10007–10024 (2014).
- ¹⁰²J. C. Dyre, "Perspective: Excess-entropy scaling," *J. Chem. Phys.* **149**, 210901 (2018).
- ¹⁰³U. R. Pedersen, L. Costigliola, N. P. Bailey, T. B. Schröder, and J. C. Dyre, "Thermodynamics of freezing and melting," *Nat. Commun.* **7**, 12386 (2016).